Geophysical Research Letters

RESEARCH LETTER
10.1029/2023GL104769

Martian Bow Shock Oscillations Driven by Solar Wind Variations: Simultaneous Observations From Tianwen-1 and MAVEN

Long Cheng[1,2,3], Robert Lillis[2], Yuming Wang[1,3], Anna Mittelholz[4], Shaosui Xu[2], David L. Mitchell[2], Catherine Johnson[5], Zhenpeng Su[1,3], Jasper S. Halekas[6], Benoit Langlais[7], Tielong Zhang[3,8,9], Guoqiang Wang[9], Sudong Xiao[9], Zhuxuan Zou[1,3], Zhiyong Wu[1,3], Yutian Chi[10], Zonghao Pan[1,3], Kai Liu[1,3], Xinjun Hao[1,3], Yiren Li[1,3], Manming Chen[1,3], Jared Espley[11], and Frank Eparvier[12]

[1]Deep Space Exploration Laboratory/School of Earth and Space Sciences, University of Science and Technology of China, Hefei, China, [2]Space Sciences Laboratory, University of California, Berkeley, Berkeley, CA, USA, [3]CAS Center for Excellence in Comparative Planetology/CAS Key Laboratory of Geospace Environment/Mengcheng National Geophysical Observatory, University of Science and Technology of China, Hefei, China, [4]Department of Earth and Planetary Sciences, Harvard University, Cambridge, MA, USA, [5]Department of Earth, Ocean, and Atmospheric Sciences, University of British Columbia, Vancouver, BC, Canada, [6]Department of Physics and Astronomy, University of Iowa, Iowa City, IA, USA, [7]Laboratoire de Planétologie et Géosciences, Nantes University, University of Angers, Le Mans Université, CNRS, Nantes, France, [8]Space Research Institute, Austrian Academy of Sciences, Graz, Austria, [9]Institute of Space Science and Applied Technology, Harbin Institute of Technology, Shenzhen, China, [10]Deep Space Exploration Laboratory, Institute of Deep Space Sciences, Hefei, China, [11]NASA Goddard Space Flight Center, Greenbelt, MD, USA, [12]Laboratory for Atmospheric and Space Physics, University of Colorado, Boulder, CO, USA

Abstract The Martian bow shock stands as the first defense against the solar wind and shapes the Martian magnetosphere. Previous studies showed the correlation between the Martian bow shock location and solar wind parameters. Here we present direct evidence of solar wind effects on the Martian bow shock by analyzing Tianwen-1 and MAVEN data. We examined three cases where Tianwen-1 data show rapid oscillations of the bow shock, while MAVEN data record changes in solar wind plasma and magnetic field. The results indicate that the bow shock is rapidly compressed and then expanded during the dynamic pressure pulse in the solar wind, and is also oscillated during the IMF rotation. The superposition of variations in multiple solar wind parameters leads to more intensive bow shock oscillation. This study emphasizes the importance of joint observations by Tianwen-1 and MAVEN for studying the real-time response of the Martian magnetosphere to the solar wind.

Plain Language Summary The Martian bow shock is a standing shock wave that forms ahead of Mars due to the interaction with the solar wind, where the supersonic solar wind flow drops sharply to subsonic. The bow shock plays a crucial role in shaping the Martian magnetosphere and controlling the energy, mass, and momentum exchange between the solar wind and the Martian atmosphere. Previous research has shown that the position of Mars' bow shock is related to the solar wind. This research presents two-spacecraft observations of how the solar wind affects the Martian bow shock. By analyzing data obtained by two orbiters, Tianwen-1 and MAVEN, we find that the bow shock quickly contracts when the solar wind dynamic pressure rises or when the interplanetary magnetic field direction turns radial. When there are multiple changes in the solar wind at the same time, the bow shock moves around even more. This study shows how important it is to look at data from Tianwen-1 and MAVEN at the same time to understand how Mars' magnetosphere reacts to the solar wind.

Key Points:

- First observations of the real-time response of the Martian bow shock to changes in the upstream solar wind
- Direct evidence of the compression of the Martian bow shock under increased solar wind dynamic pressure
- Direct evidence of motion of the Martian bow shock caused by the rotation of the interplanetary magnetic field

Supporting Information:

Supporting Information may be found in the online version of this article.

Correspondence to:

R. Lillis and Y. Wang,
rlillis@berkeley.edu;
ymwang@ustc.edu.cn

Citation:

Cheng, L., Lillis, R., Wang, Y., Mittelholz, A., Xu, S., Mitchell, D. L., et al. (2023). Martian bow shock oscillations driven by solar wind variations: Simultaneous observations from Tianwen-1 and MAVEN. *Geophysical Research Letters*, *50*, e2023GL104769. https://doi.org/10.1029/2023GL104769

Received 7 JUN 2023
Accepted 15 AUG 2023

1. Introduction

Mars lacks a current-day global internally generated dipole magnetic field, but possesses heterogeneous and locally strong crustal magnetic fields (Acuña et al., 1999). This results in a unique and complex space environment formed by the interaction between the solar wind and the combined obstacle of Mars' exosphere, conducting ionosphere, and these crustal fields (Brain et al., 2017; Fränz et al., 2006; Nagy et al., 2004). Mars' magnetosphere has several recognized plasma boundaries, such as the bow shock, the magnetic pileup boundary, the

ion composition boundary, and the photo electron boundary (Garnier et al., 2017; Holmberg et al., 2019; Nagy et al., 2004). The bow shock slows down and deflects the supersonic solar wind and heats up solar wind plasma in a turbulent magnetosheath. The location and global shape of the bow shock reflect the interaction between the solar wind and Martian magnetosphere, and these vary depending on solar wind and interplanetary magnetic field (IMF) conditions (Garnier et al., 2022). The effects of the solar wind and IMF on the Martian bow shock are an essential piece in comprehending the dynamics of the Martian plasma environment.

The accumulation of magnetic field and plasma data from the Mars Global Surveyor (MGS; Albee et al., 1998), Mars Express (MEX; Chicarro et al., 2004) and Mars Atmosphere and Volatile EvolutioN (MAVEN; Jakosky et al., 2015) has enabled extensive investigations of the location and shape of the Martian bow shock (Simon Wedlund et al., 2022). Variations of bow shock locations have also been widely studied. A statistical study by Vignes et al. (2002), using the data from the magnetometer (MAG) and electron reflectometer onboard MGS, found that the distance of the bow shock terminator from the planet's center is greater for large IMF cone angles (i.e., angle between the IMF vector and Mars-Sun line) than for small cone angles in the northern hemisphere, and that the quasi-parallel-region of the bow shock is closer to the planet than the quasi-perpendicular-region. Concurrent measurements from MGS and MEX (Edberg et al., 2009b) and Rosetta and MEX (Edberg et al., 2009a) revealed that a higher dynamic pressure, P_{dyn}, causes the Martian bow shock to move inward. The result was confirmed by a statistical study using MEX data (Edberg et al., 2009a), which further revealed (a) that the IMF direction could cause the bow shock to move outward in the hemisphere with a locally upward convection electric field and (b) that an increase in solar extreme ultraviolet (EUV) flux can also cause the bow shock to move outward. Edberg et al. (2010) used the magnetosonic Mach number, M_{ms}, measured near Earth and extrapolated to Mars during a time of approximate radial alignment, and found that an increase in M_{ms} results in lower altitudes for the Martian bow shock. Hall et al. (2016) discovered that changes in the solar EUV flux have a greater impact on the location of the bow shock than variations in P_{dyn}. Hall et al. (2019) also revealed the similarity between the variation in the bow shock position and solar EUV flux over solar cycle 23–24. Research based on MAVEN observations confirmed that while the EUV and M_{ms} are the two most significant factors for the bow shock location, the solar wind P_{dyn} also plays a role (Garnier et al., 2022; Halekas et al., 2017).

Magnetohydrodynamics simulations supported this picture of the influence of solar wind M_{ms} and P_{dyn} on the location of the Martian bow shock (Wang et al., 2020b). Additionally, the simulations indicated that the subsolar standoff distance and the flaring angle, which is related to the eccentricity of the bow shock, increase with the tangential IMF components to the solar wind flow direction, while the parallel IMF component has little effect on the subsolar standoff distance but influences the flaring angle.

Recently, Garnier et al. (2022) established a hypothesis on the drivers of the location of Martian bow shock, based on a statistical analysis on MEX and MAVEN data. To mitigate the effects of the cross-correlations among the multiple potential drivers, a partial correlation analysis was employed, and the relative importance of the parameters was ranked using model selection methods. They concluded that the EUV flux and M_{ms} are the primary factors determining the shock location, with the solar wind P_{dyn} and crustal fields as secondary drivers. Additionally, the IMF direction plays a significant role, with perpendicular shocks being positioned farther from Mars than parallel shocks.

Most of the previous studies on the impacts of solar wind on the Martian bow shock were based on statistical analyses of numerous bow shock events observed by a single orbiter. However, this approach precludes the study of the response of the bow shock to solar wind and IMF changes on short timescales. The successful deployment of the Tianwen-1 mission (Wan et al., 2020), along with the simultaneous operation of the MAVEN spacecraft, enables our study on solar wind effects on the bow shock in detail. In this study, we utilize simultaneous observations from Tianwen-1 and MAVEN to investigate the real-time response of the Martian bow shock to variations in the solar wind.

2. Data

We utilize data collected by the Tianwen-1 magnetometer (MOMAG; Liu et al., 2020; Wang et al., 2023; Zou et al., 2023) from 2021 November 15 to 2021 December 31. The data set provides the three components of the magnetic field in Mars Solar Orbital (MSO) coordinates, where the X-axis points from Mars to the Sun, the Z-axis toward the north ecliptic pole, and the Y-axis completes the right-handed coordinate system, sampled at

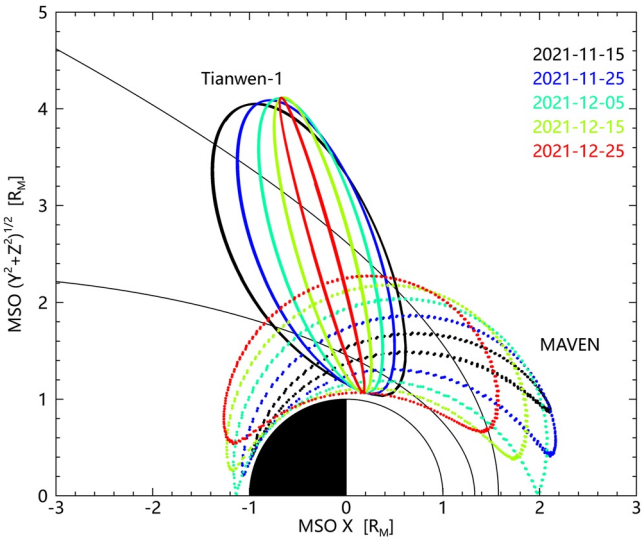

Figure 1. Orbits of Tianwen-1 and MAVEN in MSO cylindrical coordinates. The solid lines represents Tianwen-1 orbits and the dashed lines represents MAVEN orbits from 2021 Nov 15 to the end of 2021, with a cadence of 10 days. Locations of the bow shock and the magnetic pileup boundary from Edberg et al. (2008) are also shown.

1 Hz, which was its normal mode. We also incorporate data obtained from the MAVEN mission during this period, including data acquired by the magnetometer (MAG; Connerney et al., 2015), solar wind ion analyzer (SWIA; Halekas et al., 2015) and solar extreme ultraviolet monitor (EUVM; Eparvier et al., 2015) instruments. MAVEN MAG data used in the study is at the same frequency of 1 Hz with MOMAG and in MSO coordinates. SWIA fine mode data is used to calculate the physical moments of solar wind protons, such as the number density, speed, and temperature (Halekas et al., 2017). EUVM provides the solar irradiance data in 0.1–7 nm, 17–22 nm, and 121–122 nm bands; to ensure the appropriate quality of the data, we only use observations when the instrument's boresight is directed toward the Sun and is optimal for solar observations.

Figure 1 shows the orbit variations of Tianwen-1 and MAVEN spacecraft in MSO cylindrical coordinates. Both Tianwen-1 and MAVEN orbits crossed the bow shock during 2021 November and December. Tianwen-1 crossed the bow shock near the terminator and MAVEN was near the nose of the bow shock when it was located in the solar wind during this period. In this context, we find bow shock multiple-crossing cases in which Tianwen-1 recorded the shock surface oscillation while MAVEN simultaneously captured data in the solar wind upstream of the bow shock. The availability of such observations makes it possible to investigate the response of the bow shock flank to the variations in the solar wind.

3. Method

We identify Tianwen-1 crossings of the bow shock by the discontinuity between the solar wind and sheath, where the magnetic field strength $|B|$ rapidly increases and becomes more disturbed from the solar wind to the sheath. While Tianwen-1 crosses the bow shock multiple times within a few minute interval, the possible drivers for the bow shock are derived from:

1. IMF strength: derived from the root-sum-squared of the three components of the magnetic field measured by the MAVEN/MAG.
2. The clock and cone angle of the IMF: the direction of the IMF is determined by the three components of the magnetic field in MSO coordinates, with the clock angle defined as $\tan^{-1}(B_y/B_z)$ and the cone angle defined as $\cos^{-1}(-B_x/|B|)$.
3. Solar wind magnetosonic Mach number (M_{ms}): M_{ms} is determined by v_{sw}/v_f, with v_{sw} the proton speed from SWIA and v_f the fast magnetosonic speed, which is calculated by $v_f^2 = 1/2\left[v_A^2 + v_{cs}^2 + \sqrt{\left(v_A^2 + v_{cs}^2\right)^2 - 4v_A^2 v_{cs}^2 \cos^2\theta}\right]$. The Alfvén speed v_A is determined by $v_A = |B|/\sqrt{\mu_0 \rho}$, where μ_0 is the vacuum magnetic permeability and the density comes from the mass and number density of the proton, $\rho = m_p n_p$. The speed of sound $v_{cs} = \sqrt{(T_e + 5/3T_p)/m_p}$; here we assume the same temperature of solar wind electrons, T_e, and protons, T_p, and take the polytropic index 1 for solar wind electrons and 5/3 for protons, considering the isothermal/adiabatic behavior of solar wind electrons/ions (Burne et al., 2021; Halekas et al., 2017). θ is the angle between the wave propagation and the magnetic field; here we use the cone angle, which results in v_f along the MSO X axis.
4. Solar wind dynamic pressure (P_{dyn}): $P_{dyn} = \rho v_{sw}^2$.
5. Angle between the bow shock normal and IMF (θ_{Bn}): the key parameter is the bow shock normal, which is estimated by two methods in this study. The first method is to apply the minimum variances analysis (MVA; Sonnerup & Scheible, 1998) to a series of magnetic field data taken over a 5-min time window centered on the crossing time. The shock normal is the direction along which the magnetic field varies minimally, as the magnetic field remain the shock normal should keep constant when crossing the shock surface. The second method is to utilize the shock normal from the bow shock model. When the spacecraft is close to the bow shock, we first find the point on the shock surface that is closest to the spacecraft and derive the normal at that point from the bow shock model (Schwartz, 1998; Simon Wedlund et al., 2022).

EUV irradiance is also one of the primary factors affecting the location of the Martian bow shock, however, the duration of every case in this study is limited to tens of minutes, during which the EUV irradiance remained constant and we have opted not to present the EUV data in this study.

As the magnetic field measured by MOMAG and MAG are both utilized in this study, we first provide detailed comparisons of the IMF measured by the two spacecraft and the reasonability of using MAG as the monitor of upstream IMF for Tianwen-1 in Supporting Information S1.

4. Results

Here we looks at three case studies, where the first two are more straightforward and clean and show the result of single parameter effect, while the last case is more typical and shows the result of multiple parameters affecting the bow shock location.

4.1. Shock Oscillation Controlled by the Solar Wind Dynamic Pressure

Figure 2 reveals the Martian bow shock motion in response to a solar wind transient with a dynamic pressure spike. Between 07:00UT and 07:20UT on 2021 November 30, Tianwen-1 moved from the sheath to the solar wind near the terminator, while MAVEN stayed in the upstream solar wind near the bow shock nose (Figures 2h and 2i). Figures 2a and 2b show the magnetic field strength and vectors from Tianwen-1 MOMAG. In general, $|B|$ decreases from ∼7 nT in the sheath to ∼2 nT in the solar wind, which is close to the IMF strength measured by MAVEN (Figure 2c). Tianwen-1 was immersed in the solar wind after 07:11UT (t_3, marked by the third vertical dashed line), with $|B|$ rapidly decreasing and then stabilizing. Before Tianwen-1 fully left the sheath, its $|B|$ dropped quickly at 07:07UT (t_1) and then returned to the sheath level at 07:08UT (t_2). Between t_1 and t_2, the value of $|B|$ nearly decreased to the solar wind level, ∼2 nT; the IMF strength, the clock and cone angle were stable at ∼2 nT, −90° and 135° respectively, as measured by MAVEN in the upstream solar wind (Figures 2c–2e)).

It is noteworthy that the solar wind P_{dyn} quickly increased and stayed at high level for ∼1 min right before t_1, which was caused by the solar wind density variation (not shown). We infer that the sudden increase of P_{dyn} from ∼0.65 to ∼0.75 nPa compressed the bow shock at t_1, causing Tianwen-1 to be briefly exposed to the solar wind, leading to the rapid decrease in $|B|$. Subsequently, when P_{dyn} decreased to ∼0.65 nPa at t_2, the bow shock expanded again, resulting for Tianwen-1 to be back into the sheath where $|B|$ recovered to the sheath level. During the period of interest from 07:00 to 07:20 UT, M_{ms} continuously fluctuated between the values of about 6 and 8. Corresponding to the peak of P_{dyn} before t1, M_{ms} exhibited three spikes; considering the significant impact of Mms on the shock location, the varying M_{ms} might also play a role in this event.

Figure 2j illustrates the distance along the shock normal between the shock locations at t_1 and t_3 is ∼0.07 R_M. Obviously, the actual spatial oscillation is probably larger than this scale. Hence, the 0.1 nPa perturbation of P_{dyn} in this event caused the bow shock motion at a scale >250 km along the shock normal. Overall, the locations of the bow shocks in this event are closer to the planet compared with Edberg's model, which may be due to the high M_{ms} and the quasi-parallel shock.

4.2. Shock Oscillation Controlled by the IMF

During 03:50UT to 04:15UT on 2021 Dec 26, Tianwen-1 observed an oscillation of the bow shock that may be caused by an IMF transient with a radialward rotation. At the beginning of the event, Tianwen-1 was in the solar wind with $|B|$ at ∼3 nT. As Tianwen-1 entered the sheath, the magnetic field became highly variable with |B| increasing at ∼03:56UT (t_1) and $|B|$ increased to ∼10 nT at ∼04:00UT. At 04:07UT (t_2), $|B|$ decreased rapidly back to ∼3 nT, close to the IMF strength measured by MAVEN. Then $|B|$ increased rapidly to the sheath level again at ∼04:10UT (t_3).

During t_2 and t_3, there was no significant change in the solar wind M_{ms} and P_{dyn}, and the IMF strength was also stable; however, the IMF direction changed considerably; the clock angle shifted from −90° to −180° (denoting a change from westward IMF to southward IMF), the cone angle shifted from 150° to 180°. Cone and clock angles both returned to their original values within ∼2.5 min. Thus, the IMF direction before and after the transient is Parker-spiral-like, while during the transient, it became radial and directed toward the Sun. The begin and end

10.1029/2023GL104769

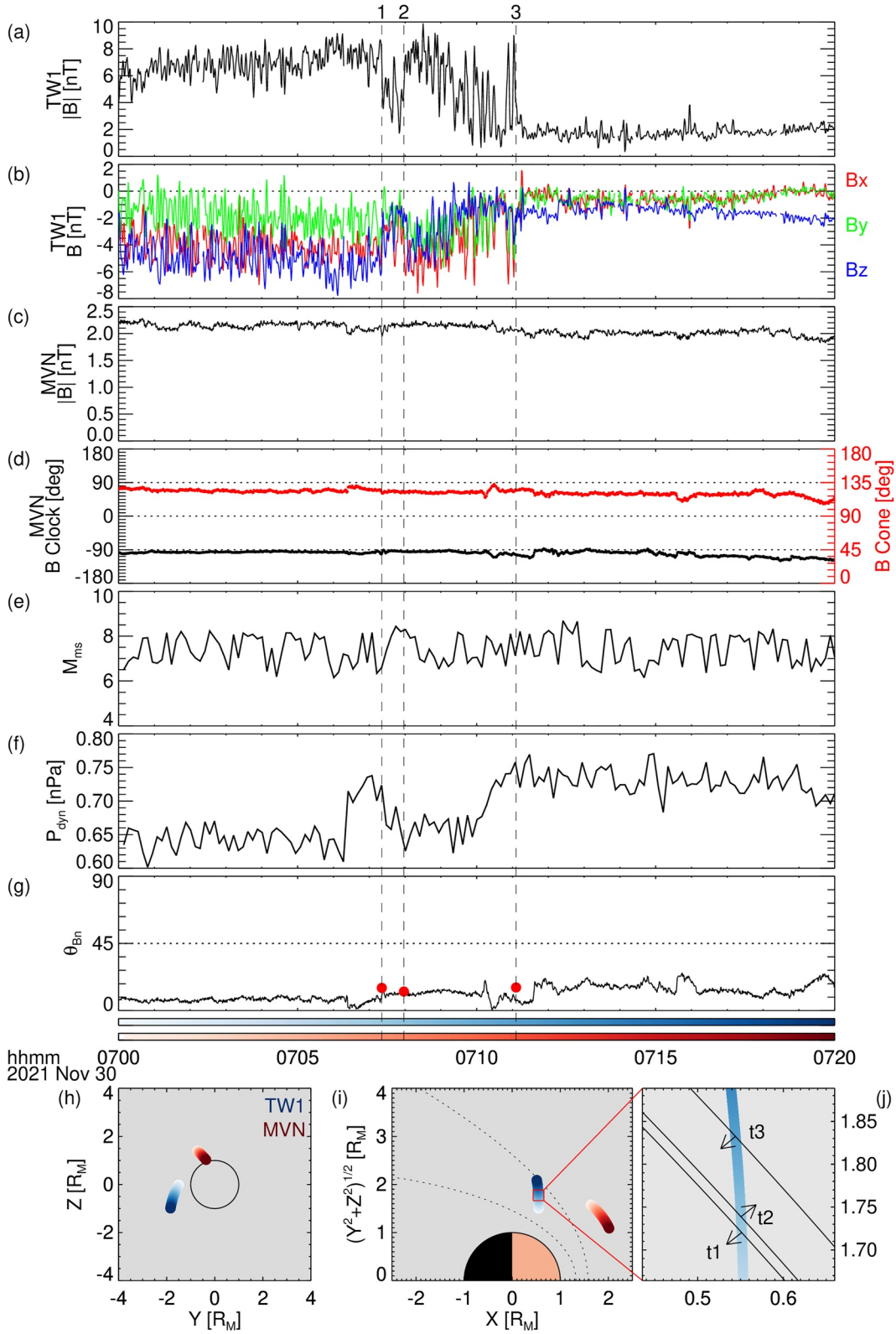

Figure 2.

times of the transient are ∼1 min before t_2 and t_3, respectively, well corresponding to the crossing of the bow shock. Hence, we infer that the temporarily radial IMF caused the bow shock to move inward; after the transient has passed, the bow shock may expand back toward its original position (Figure 3j).

For the Earth bow shock, Wang et al. (2020a) found that under the radial IMF condition, the dayside of the bow shock is located closer to the Earth than the average. For the Martian bow shock, Sui et al. (2023) found that the subsolar and flank regions of the Martian bow shock are situated closer to Mars under the radial IMF condition, which is consistent with our result. In addition, the varying IMF direction changes θ_{Bn} of the shock. In this event, the local θ_{Bn} changed from ∼90° to ∼45°, which may also cause the inward motion of the bow shock. For this event, maybe only a portion of the bow shock moves inward, since different parts of the bow shock may undergo different θ_{Bn} changes and thus move in different directions.

4.3. Shock Oscillation Controlled by Multiple Factors

While the prior two cases demonstrated bow shock oscillations driven by P_{dyn} pulse and IMF rotation separately, we have identified more complex events, in which Tianwen-1 observed bow shock oscillations accompanied by changes in several parameters of the solar wind measured by MAVEN.

Figure 4 shows one such example, a multiple shock crossing event observed by Tianwen-1 between 00:55UT and 01:30UT on 2021 Dec 09. As |*B*| recorded by MOMAG fluctuates between the solar wind level (∼3 nT) and the sheath level (∼10 nT), Tianwen-1 crosses the bow shock 5 times at cadences of several minutes, entering the sheath at ∼01:11UT (t_1, as marked by the first vertical line in Figure 4), ∼01:13UT (t_3), ∼01:23UT (t_5) and entering the solar wind at ∼01:12UT (t_2) and ∼01:16UT (t_4). Highly variable upstream solar wind conditions monitored by MAVEN may be linked to the bow shock's motion. Approximately 1 min before t_4, the IMF strength quickly decreased from ∼4.5 to ∼3 nT, while the dynamic pressure increased from ∼1.2 to ∼1.5 nPa, returning to the previous level ∼1 min before t_5. These changes may have contributed to the bow shock motion detected by Tianwen-1 at t_4 and t_5. The oscillation between t_1 and t_3 may have been caused by the increasing of the IMF strength and decreasing of the dynamic pressure at ∼01:09 UT. The increase in amplitude and fluctuation of the magnetic field at ∼01:04 UT may be due to the approach of Tianwen-1 to the bow shock caused by shock expansion caused by the increasing IMF strength, rapid rotation of IMF, and the decreasing dynamic pressure at ∼01:03 UT. With the quick rotation of the IMF at ∼01:08 UT, the bow shock may have shrunk, making Tianwen-1 away from the bow shock, and causing |B| measured by MOMAG to return to the amplitude and fluctuation of the solar wind level.

5. Conclusions and Discussions

In this study, we provide direct evidence of solar wind effects on Martian bow shock oscillations using simultaneous observations from Tianwen-1 and MAVEN. We present three cases where Tianwen-1 crossed the bow shock multiple times within a few minutes interval, while MAVEN stayed in the upstream solar wind. During the motion of bow shock observed by Tianwen-1/MOMAG, MAVEN monitored the changes in solar wind parameters, like the IMF strength and direction, M_{ms} and P_{dyn}. Through these observations, we are able to establish direct connections between the bow shock oscillations and the solar wind fluctuations. The case in Section 4.1 shows direct evidence of P_{dyn} modulations on the position of Martian bow shock. The shrinking and expanding of the bow shock may be mainly caused by the P_{dyn} pulse. The case in Section 4.2 shows direct evidence of IMF direction modulations on the bow shock position. The shrink of the bow shock near the spacecraft may be caused by the radial IMF or by the turning from the quasi-perpendicular shock to oblique shock. The case in Section 4.3 shows the complicated modulation of various changing parameters in the solar wind on the bow

Figure 2. Observations from 07:00 to 07:20 UT on 2021 November 30, including Tianwen-1 observations of (a) the magnetic field strength and (b) the three components of the magnetic field in Mars Solar Orbital (MSO) coordinates, MAVEN observations of (c) the magnetic field strength, (d) directions of the magnetic field in MSO coordinates, including the clock angle (black line) and cone angle (red line), (e) the magnetosonic Mach number, M_{ms}, (f) the solar wind dynamic pressure, P_{dyn}, and (g) the angel between the interplanetary magnetic field and the shock normal, which are derived from the bow shock model (black line) and minimum variance analysis method (red points). The bottom row of panels shows the Tianwen-1 and MAVEN orbits in panel (h) the *Y*–*Z* plane, as viewed from the Sun, and (i) aberrated-MSO cylindrical coordinates. Locations of the bow shock and the magnetic pileup boundary from Edberg et al. (2008) are shown for reference (dotted lines). (j) is the zoom-in plot for the region marked by the red box in (i), where solid conic lines show locations of the scaled bow shocks observed by Tianwen-1 (Sonnerup & Scheible, 1998), and arrows show the inferred moving directions of the bow shock. The dashed vertical lines over (a) to (g) show the time for Tianwen-1 bow shock crossings.

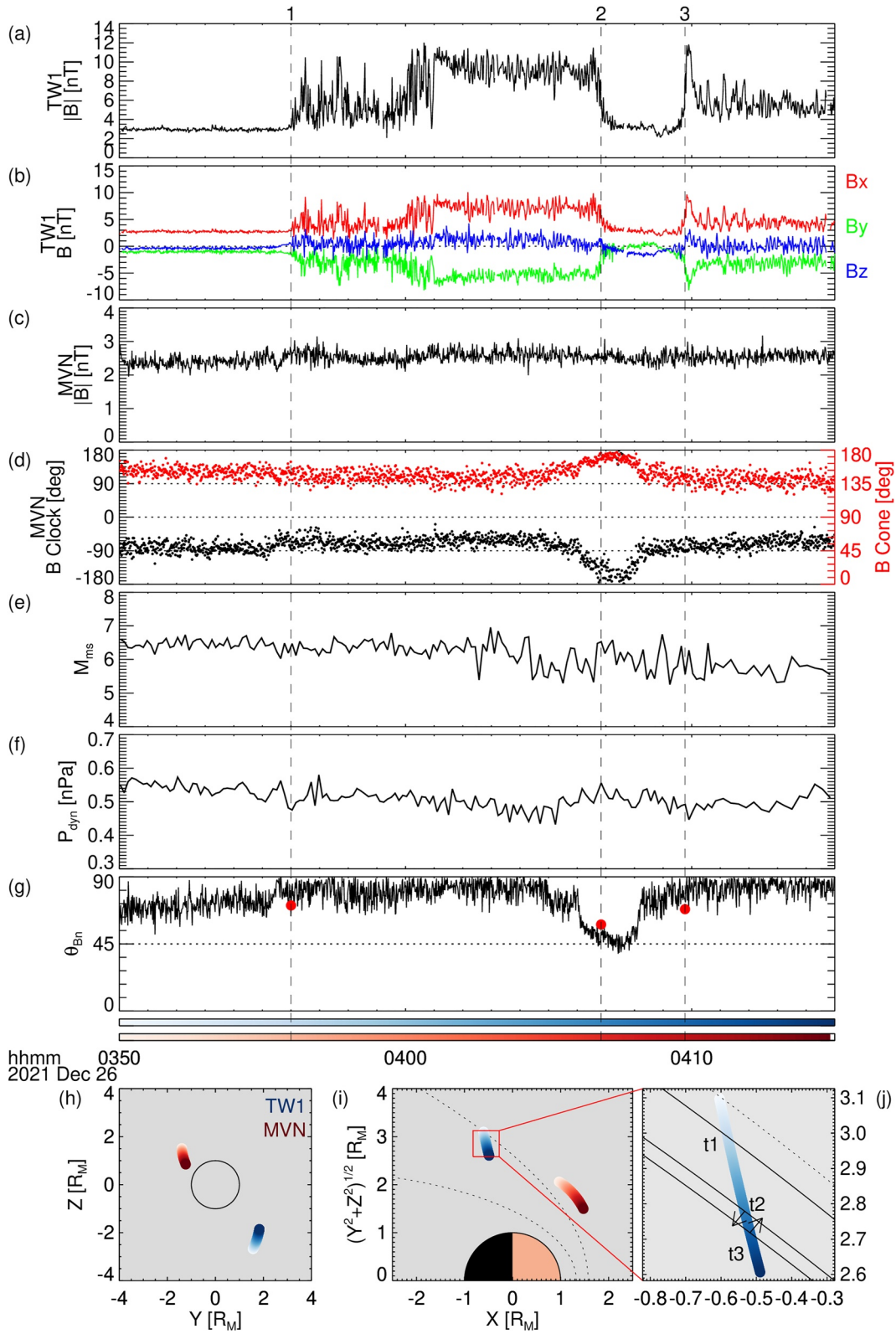

Figure 3. Similar to Figure 2 but for the case that Tianwen-1 observed the bow shock oscillation caused by the temporary radialward turning of interplanetary magnetic field direction between 03:50UT and 04:15UT on 2021 December 26.

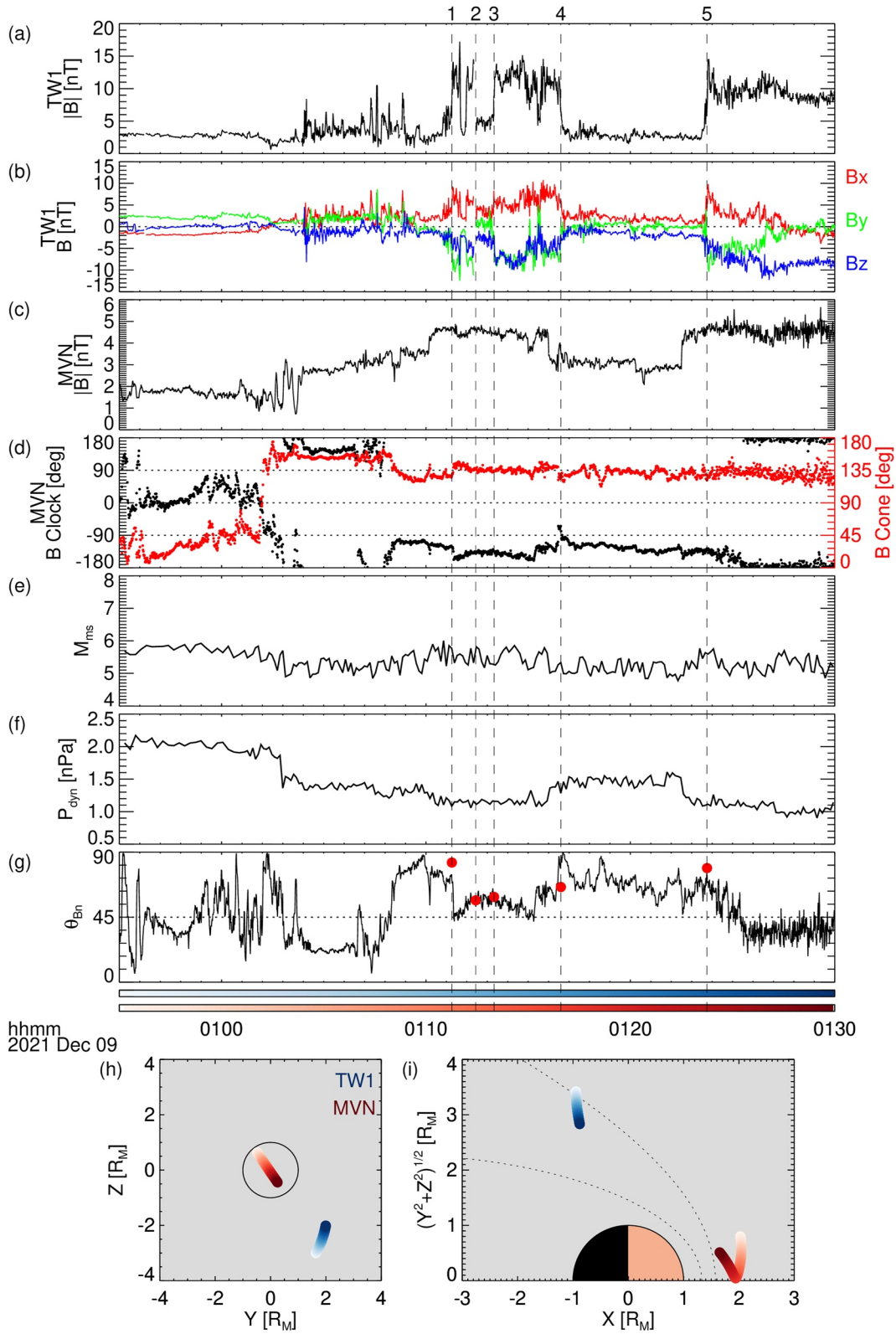

Figure 4. Similar to Figure 2 but for the case that Tianwen-1 observed the bow shock oscillation under solar wind transients with multiple varying parameters, between 00:55UT and 01:30UT on 2021 December 9.

shock location. The increases of P_{dyn}, M_{ms} or IMF strength, or radial IMF, can compress the Martian bow shock individually. When these factors are combined at different times, their superposition make the bow shock motions more frequent and rapid.

The time delay between the time when MAVEN detected changes in the solar wind and the time when Tianwen-1 crossed the moving bow shock later is noteworthy. It may be is a function of several factors: (a) the propagation time of the solar wind from MAVEN to the bow shock, (b) the response time of the bow shock to solar wind changes, and (c) the propagation time of the bow shock from its original position to where it crossed by Tianwen-1. The first factor, the propagation time of the solar wind, can be estimated by the distance of two spacecraft in MSO X direction and the solar wind speed, which is about 10–15 s in the first and second event. Taking out the solar wind propagation time, there is still a ∼1-min time. The exact value of the response time is unknown, but must be less than 1 min. It reveals the rapid response of the bow shock to the solar wind variation, which is consistent with the simulations (Ma et al., 2014; Song et al., 2023). For the second event, if we assume that the bow shock kept static before the IMF rotation and responded to the solar wind instantaneously, after removing the propagation time of the solar wind, the ∼1-min time difference between IMF rotation and t_2 would be the time needed for the bow shock to move from bow shock location at t_1 to that at t_2. The distance along the normal, between the two locations, is ∼0.12 R_M (Figure 3j). The mean shock speed along the normal is estimated to be ∼7 km/s. If we assume that the bow shock underwent a uniformly accelerated motion, its speed at t_2 is estimated to be ∼14 km/s.

Data Availability Statement

The MAVEN data is publicly available at NASA's Planetary Data System (https://pds-ppi.igpp.ucla.edu/mission/MAVEN). Tianwen-1/MOMAG data is available at the Lunar and Planetary Data Release System (https://moon.bao.ac.cn/web/enmanager/kxsj?missionName=HX1&zhName=MOMAG&grade=2C). The MOMAG data used in this letter could also be retrieved from the official site of the MOMAG team (http://space.ustc.edu.cn/dreams/tw1_momag/).

Acknowledgments
We are grateful to all the individuals and teams who provide the calibrated data used in this study. The authors from USTC are supported by the grants from NSFC (42130204 and 42188101) and the Strategic Priority Program of CAS (XDB41000000). We thank the helpful comments by P. Garnier and another anonymous reviewer. L.C. thanks the support of the Excellent Doctoral Overseas Study Program of USTC. Y.W. is particularly grateful for the support of the Tencent Foundation.

References

Acuña, M. H., Connerney, J. E. P., Ness, N. F., Lin, R. P., Mitchell, D., Carlson, C. W., et al. (1999). Global distribution of crustal magnetization discovered by the Mars Global Surveyor MAG/ER experiment. *Science*, *284*(5415), 790–793. https://doi.org/10.1126/science.284.5415.790

Albee, A. L., Palluconi, F. D., & Arvidson, R. E. (1998). Mars global surveyor mission: Overview and status. *Science*, *279*(5357), 1671–1672. https://doi.org/10.1126/science.279.5357.1671

Brain, D. A., Barabash, S., Bougher, S. W., Duru, F., Jakosky, B. M., & Modolo, R. (2017). Solar wind interaction and atmospheric escape. In *The atmosphere and climate of Mars* (pp. 464–496). Cambridge University Press. https://doi.org/10.1017/9781139060172.015

Burne, S., Bertucci, C., Mazelle, C., Morales, L. F., Meziane, K., Halekas, J., et al. (2021). The structure of the Martian quasi-perpendicular supercritical shock as seen by MAVEN. *Journal of Geophysical Research: Space Physics*, *126*(9), e2020JA028938. https://doi.org/10.1029/2020JA028938

Chicarro, A., Martin, P., & Trautner, R. (2004). *The Mars express mission: An overview*. ESA Special Publication.

Connerney, J. E. P., Espley, J., Lawton, P., Murphy, S., Odom, J., Oliversen, R., & Sheppard, D. (2015). The MAVEN magnetic field investigation. *Space Science Reviews*, *195*(1–4), 257–291. https://doi.org/10.1007/s11214-015-0169-4

Edberg, N. J. T., Auster, U., Barabash, S., Bößwetter, A., Brain, D. A., Burch, J. L., et al. (2009a). Rosetta and Mars express observations of the influence of high solar wind pressure on the Martian plasma environment. *Annales Geophysicae*, *27*(12), 4533–4545. https://doi.org/10.5194/angeo-27-4533-2009

Edberg, N. J. T., Brain, D. A., Lester, M., Cowley, S. W. H., Modolo, R., Fränz, M., & Barabash, S. (2009b). Plasma boundary variability at Mars as observed by Mars global surveyor and Mars express. *Annales Geophysicae*, *27*(9), 3537–3550. https://doi.org/10.5194/angeo-27-3537-2009

Edberg, N. J. T., Lester, M., Cowley, S. W. H., Brain, D. A., Fränz, M., & Barabash, S. (2010). Magnetosonic Mach number effect of the position of the bow shock at Mars in comparison to Venus. *Journal of Geophysical Research*, *115*(A7), A07203. https://doi.org/10.1029/2009ja014998

Edberg, N. J. T., Lester, M., Cowley, S. W. H., & Eriksson, A. I. (2008). Statistical analysis of the location of the Martian magnetic pileup boundary and bow shock and the influence of crustal magnetic fields. *Journal of Geophysical Research*, *113*(8), A08206. https://doi.org/10.1029/2008JA013096

Eparvier, F. G., Chamberlin, P. C., Woods, T. N., & Thiemann, E. M. B. (2015). The solar extreme ultraviolet monitor for MAVEN. *Space Science Reviews*, *195*(1–4), 293–301. https://doi.org/10.1007/s11214-015-0195-2

Fränz, M., Dubinin, E., Roussos, E., Woch, J., Winningham, J. D., Frahm, R., et al. (2006). Plasma moments in the environment of Mars: Mars express ASPERA-3 observations. *Space Science Reviews*, *126*(1–4), 165–207. https://doi.org/10.1007/s11214-006-9115-9

Garnier, P., Jacquey, C., Gendre, X., Genot, V., Mazelle, C., Fang, X., et al. (2022). The drivers of the Martian bow shock location: A statistical analysis of Mars atmosphere and volatile EvolutioN and Mars express observations. *Journal of Geophysical Research: Space Physics*, *127*(5), e2021JA030147. https://doi.org/10.1029/2021JA030147

Garnier, P., Steckiewicz, M., Mazelle, C., Xu, S., Mitchell, D., Holmberg, M. K. G., et al. (2017). The Martian photoelectron boundary as seen by MAVEN. *Journal of Geophysical Research: Space Physics*, *122*(10), 10472–10485. https://doi.org/10.1002/2017JA024497

Halekas, J. S., Ruhunusiri, S., Harada, Y., Collinson, G., Mitchell, D. L., Mazelle, C., et al. (2017). Structure, dynamics, and seasonal variability of the Mars-solar wind interaction: MAVEN solar wind ion analyzer in-flight performance and science results. *Journal of Geophysical Research: Space Physics*, *122*(1), 547–578. https://doi.org/10.1002/2016JA023167

Halekas, J. S., Taylor, E. R., Dalton, G., Johnson, G., Curtis, D. W., McFadden, J. P., et al. (2015). The solar wind ion analyzer for MAVEN. *Space Science Reviews*, *195*(1), 125–151. https://doi.org/10.1007/s11214-013-0029-z

Hall, B. E. S., Lester, M., Sánchez-Cano, B., Nichols, J. D., Andrews, D. J., Edberg, N. J. T., et al. (2016). Annual variations in the Martian bow shock location as observed by the Mars express mission. *Journal of Geophysical Research: Space Physics*, *121*(11), 11474–11494. https://doi.org/10.1002/2016JA023316

Hall, B. E. S., Sánchez-Cano, B., Wild, J. A., Lester, M., & Holmström, M. (2019). The Martian bow shock over solar cycle 23–24 as observed by the Mars express mission. *Journal of Geophysical Research: Space Physics*, *124*(6), 4761–4772. https://doi.org/10.1029/2018JA026404

Holmberg, M. K. G., André, N., Garnier, P., Modolo, R., Andersson, L., Halekas, J., et al. (2019). MAVEN and MEX multi-instrument study of the dayside of the Martian induced magnetospheric structure revealed by pressure analyses. *Journal of Geophysical Research: Space Physics*, *124*(11), 8564–8589. https://doi.org/10.1029/2019JA026954

Jakosky, B. M., Lin, R. P., Grebowsky, J. M., Luhmann, J. G., Mitchell, D. F., Beutelschies, G., et al. (2015). The mars atmosphere and volatile evolution (MAVEN) mission. *Space Science Reviews*, *195*(1–4), 3–48. https://doi.org/10.1007/s11214-015-0139-x

Liu, K., Hao, X. J., Li, Y. R., Zhang, T. L., Pan, Z. H., Chen, M. M., et al. (2020). Mars orbiter magnetometer of China's first Mars mission Tianwen-1. *Earth and Planetary Physics*, *4*(4), 384–389. https://doi.org/10.26464/epp2020058

Ma, Y. J., Fang, X., Nagy, A. F., Russell, C. T., & Toth, G. (2014). Martian ionospheric responses to dynamic pressure enhancements in the solar wind. *Journal of Geophysical Research: Space Physics*, *119*(2), 1272–1286. https://doi.org/10.1002/2013JA019402

Nagy, A. F., Winterhalter, D., Sauer, K., Cravens, T. E., Brecht, S., Mazelle, C., et al. (2004). The plasma environment of Mars. *Space Science Reviews*, *111*(1–2), 33–114. https://doi.org/10.1023/B:SPAC.0000032718.47512.92

Schwartz, S. J. (1998). Shock and discontinuity normals, Mach numbers, and related parameters. In *ISSI Scientific Report Series* (Vol. 1, pp. 249–270).

Simon Wedlund, C., Volwerk, M., Beth, A., Mazelle, C., Möstl, C., Halekas, J., et al. (2022). A fast bow shock location predictor-estimator from 2D and 3D analytical models: Application to Mars and the MAVEN mission. *Journal of Geophysical Research: Space Physics*, *127*(1), e2021JA029942. https://doi.org/10.1029/2021JA029942

Song, Y., Lu, H., Cao, J., Li, S., Yu, Y., Wang, S., et al. (2023). Effects of force in the Martian plasma environment with solar wind dynamic pressure enhancement. *Journal of Geophysical Research: Space Physics*, *128*(3), e2022JA031083. https://doi.org/10.1029/2022JA031083

Sonnerup, B. U. O., & Scheible, M. (1998). Minimum and maximum variance analysis. In *Analysis methods for multi-spacecraft data* (pp. 185–220).

Sui, H. Y., Wang, M., Lu, J. Y., Zhou, Y., & Wang, J. (2023). Interplanetary magnetic field effect on the location of the Martian bow shock MAVEN observations. *The Astrophysical Journal*, *945*(2), 136. https://doi.org/10.3847/1538-4357/acbd4c

Vignes, D., Acuna, M. H., Crider, D. H., Connerney, J., Reme, H., & Mazelle, C. (2002). Factors controlling the location of the bow shock at Mars. *Geophysical Research Letters*, *29*(9), 1–4. https://doi.org/10.1029/2001gl014513

Wan, W. X., Wang, C., Li, C. L., & Wei, Y. (2020). China's first mission to Mars. *Nature Astronomy*, *4*(7), 721. https://doi.org/10.1038/s41550-020-1148-6

Wang, M., Lu, J. Y., Kabin, K., Yuan, H. Z., Zhou, Y., & Guan, H. Y. (2020a). Influence of the interplanetary magnetic field cone angle on the geometry of bow shocks. *The Astronomical Journal*, *159*(5), 227. https://doi.org/10.3847/1538-3881/ab86a7

Wang, M., Xie, L., Lee, L. C., Xu, X. J., Kabin, K., Lu, J. Y., et al. (2020b). A 3D parametric Martian bow shock model with the effects of Mach number, dynamic pressure, and the interplanetary magnetic field. *The Astrophysical Journal*, *903*(2), 125. https://doi.org/10.3847/1538-4357/abbc04

Wang, Y., Zhang, T., Wang, G., Xiao, S., Zou, Z., Cheng, L., et al. (2023). The Mars orbiter magnetometer of Tianwen-1: In-flight performance and first science results. *Earth and Planetary Physics*, *7*(2), 1–13. https://doi.org/10.26464/epp2023028

Zou, Z., Wang, Y., Zhang, T., Wang, G., Xiao, S., Pan, Z., et al. (2023). In-flight calibration of the magnetometer on the Mars orbiter of Tianwen-1. *Science China Technological Sciences*, *66*(8), 2396–2405. https://doi.org/10.1007/s11431-023-2401-2